Near-Infrared Photoluminescence in the Femtosecond Time Region in Monolayer Graphene on SiO_2

Takeshi Koyama,[†,*] Yoshito Ito,[‡] Kazuma Yoshida,[‡] Masaharu Tsuji,[‡,§] Hiroki Ago,[‡,§] Hideo Kishida,[†] and Arao Nakamura[†,∥]

[†]Department of Applied Physics, Graduate School of Engineering, Nagoya University, Chikusa, Nagoya 464-8603, Japan, [‡]Graduate School of Engineering Sciences, Kyushu University, Kasuga, Fukuoka 816-8580, Japan, and [§]Institute for Materials Chemistry and Engineering, Kyushu University, Kasuga, Fukuoka 816-8580, Japan. [∥]Present address: Toyota Physical and Chemical Research Institute, Nagakute, Aichi 480-1192, Japan.

ABSTRACT We investigate the dynamical properties of photoexcited carriers in a single monolayer of graphene at room temperature in air using femtosecond time-resolved luminescence spectroscopy. The luminescence kinetics are observed in the near-infrared region of 0.7−1.4 eV and analyzed based on the two-temperature model describing the cooling of thermalized carriers *via* the carrier−optical phonon interaction. The observed luminescence in the range 0.7−0.9 eV is well reproduced by the model. In the range 1.0−1.4 eV, however, the luminescence, which decays in ∼300 fs, cannot be reproduced by this model. These results indicate that the carrier system is not completely thermalized in ∼300 fs. We also show the importance of the carrier-doping effect induced by the substrate and surrounding environment in the carrier cooling dynamics and the predominance of optical phonons over acoustic phonons in the carrier−phonon interactions even at a temperature of ∼400 K.

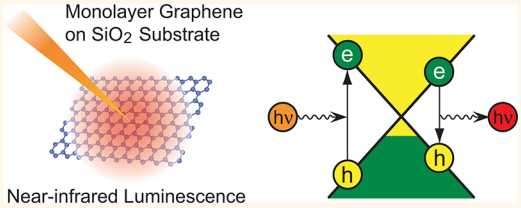

KEYWORDS: monolayer graphene · photocarrier relaxation · carrier cooling dynamics · carrier−phonon interaction · photoluminescence · femtosecond time-resolved luminescence spectroscopy

Graphene has unique conduction and valence bands with linear dispersion that contact each other at the K and K′ points of the Brillouin zone. Owing to its linear dispersion bands, graphene shows extremely intriguing electronic and optical properties.[1−5] Carrier relaxation in such linear dispersion bands has attracted significant attention. Recent experiments[6−23] and theoretical studies[24−27] have shown that photoexcitation between the linear dispersion bands initially creates nonequilibrium carriers, which experience ultrafast thermalization *via* carrier−carrier and carrier−phonon scattering followed by cooling with emission of phonons. The key to the application of graphene materials to available optoelectronic devices such as photoemitters and photosensors is a fundamental understanding of the ultrafast dynamics of carrier relaxation in graphene at low photoexcitation densities in ambient environments.

Transient absorption (pump−probe) measurements in the visible region for solution-phase chemically exfoliated graphene (probe energy, 1.57 eV),[10] for stacked graphene films (∼1.9−3.3 eV),[18] and for monolayer exfoliated graphene (∼1.3−1.8 eV)[22] have shown that ultrafast cooling of the carrier system takes place with emission of optical phonons. A similar cooling mechanism was observed using time-resolved luminescence measurements in the visible−near-ultraviolet region (1.7−3.5 eV) for monolayer exfoliated graphene.[15] On the other hand, the importance of the interaction of carriers with acoustic phonons for carrier cooling was pointed out by several groups. Pump−probe measurements in the infrared region (∼0.5−0.8 eV) for multilayer epitaxial graphene showed that cooling of the carrier system occurs initially *via* optical phonons and later *via* acoustic phonons.[19] In optical-pump terahertz-probe (∼4 meV) measurements for epitaxial graphene samples with 14 and 30 layers, cooling due to interactions of carriers with both optical and acoustic phonons was observed.[21] Theoretically, it is shown that acoustic phonons play a dominant role in carrier cooling at carrier temperatures below ∼200−300 K, while optical phonon emission dominates the cooling process at

* Address correspondence to koyama@nuap.nagoya-u.ac.jp.

Received for review November 30, 2012 and accepted February 27, 2013.

Published online March 05, 2013
10.1021/nn305558r

temperatures above this range.[28,29] Therefore, in order to understand the carrier cooling process, it is important to experimentally investigate carrier dynamics at carrier temperatures around several hundreds of Kelvin. For this purpose, we need to observe the optical response in the near-infrared region, where dynamics of low-energy carriers are directly involved. However, only a few studies in this regard have been reported, and in one specific study the transient absorption data measured at 1.88 μm were analyzed by the acoustic phonon cooling process.[19]

Recently, a carrier doping effect in graphene prepared on substrates has attracted attention; carrier doping is of great importance for applications in electronic and optical devices. Depending on the substrate material and surrounding environment (gases and chemicals), such graphene samples exhibit either an n-doped[7,30,31] or p-doped characteristic.[31−34] As optical transitions in graphene are governed by electron- and hole-distribution functions, a change in the Fermi energy by carrier doping is crucial for optical properties. Though many time-resolved measurements of the optical transition have been carried out for graphene formed on different substrates, carrier doping from the substrate material has not been given much consideration thus far.[7,17,19,21,23,35]

In this paper, we report the carrier dynamics in single-monolayer graphene on an SiO_2 substrate at room temperature in air investigated by means of femtosecond time-resolved luminescence spectroscopy. The luminescence kinetics in the infrared region of 0.7−1.4 eV show an increase in the decay time with decreasing photon energy, suggesting cooling of the photoexcited carriers. The luminescence kinetics are analyzed based on the two-temperature model of thermalized carriers, taking into account the carrier−phonon interaction and the Fermi energy shift by carrier doping from the substrate. The observed luminescence in the range 0.7−0.9 eV is well reproduced by the model, while the luminescence that decays in 300 fs in the range 1.0−1.4 eV cannot be reproduced by this model. These results indicate that the carrier system is not completely thermalized at the early stages at times shorter than ∼300 fs. Our analysis showed that the carrier cooling dynamics is governed by carrier−optical phonon interactions, and therefore acoustic phonons are irrelevant to carrier cooling at a temperature of ∼400 K. We also find the importance of the carrier-doping effect on the carrier cooling dynamics; the carrier doping suppresses a rise in carrier temperature by optical excitations due to the larger heat capacity of carriers.

RESULTS AND DISCUSSION

The graphene used in this study was epitaxially grown on Cu(111)/sapphire by chemical vapor deposition (CVD)[36−38] and then transferred onto an SiO_2 (quartz) substrate. The obtained graphene had dimensions of ∼20 mm × 20 mm. Raman scattering measurements were carried out for characterizing the graphene samples. Figure 1a shows the typical Raman spectrum of the graphene in this study at room temperature in air. Three bands are observed at ∼1320, ∼1590, and ∼2640 cm^{-1}, which are assigned to the D, G, and 2D bands, respectively.[39] The G and D bands are associated with the zone-center (Γ point) longitudinal and zone-boundary (K point) transverse optical phonons, respectively; the D band is activated in the first-order Raman process by the presence of defects. The 2D band is due to second-order Raman scattering of the K-point transverse optical phonons. The spectral weight of the D band is small in the observed Raman spectra, indicating that the graphene is free of a large number of defects and its crystalline quality is high.

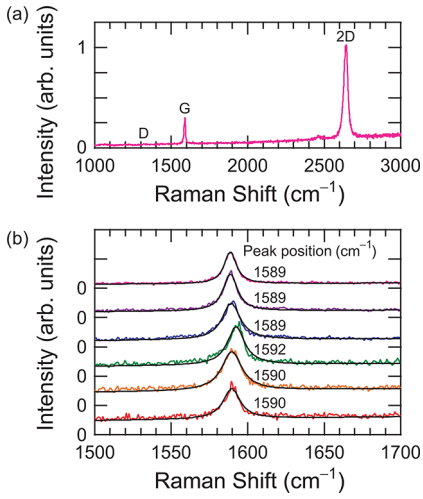

Figure 1. (a) Typical Raman spectrum for the monolayer graphene sample at room temperature in air. (b) Raman spectra measured at six different points separated from each other by ∼2 mm around the center of the sample. The baselines are shifted for display clarity. The black solid lines represent the results of curve fitting with a Lorentz function and a linear background component, and the peak position of the Lorentz function in the respective curves is indicated in the figure.

The number of stacked graphene layers can be determined from the peak intensity ratio of the 2D band to the G band (I_{2D}/I_G):[40,41] $I_{2D}/I_G \approx 2-5$ and 1 for monolayer and bilayer graphene, respectively. Since the observed Raman spectra in Figure 1a show that $I_{2D}/I_G \approx 3.5$, the graphene used in this study is identified to be monolayer graphene. This identification is supported by the sharp spectral shape of the 2D band compared with that for multilayer graphene.[40,41]

The peak position of the G band is sensitive to the charge carrier density, *i.e.*, the Fermi energy shift ΔE_F, in graphene. Raman scattering measurements for monolayer graphene with an applied electric field show the linear dependence of the G-band frequency on the electric-field-effect-modulated Fermi energy.[42]

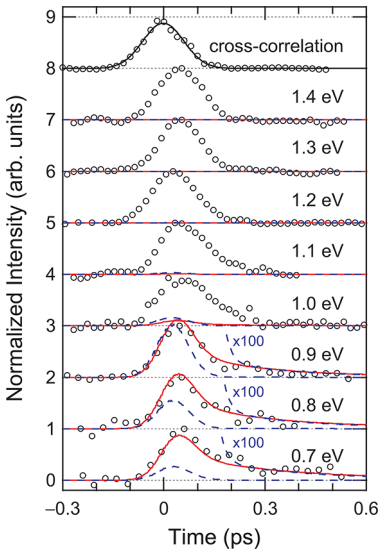

Figure 2. Luminescence kinetics in monolayer graphene in the photon energy range 0.7−1.4 eV at room temperature in air. For clarity of display, the baselines are shifted and the intensities are normalized at the maxima. The circle symbols represent experimental data, and the red solid and blue dashed curves are the results of calculations based on a two-temperature model with and without a Fermi energy shift, respectively. The top curve represents the cross-correlational trace between the gate pulse and excitation pulse, which gives the instrument response function. This curve has a Gaussian shape with a full width at half-maximum of 140 fs (black solid line).

The substrate-mediated strain in graphene also gives rise to a peak shift of the G band depending on the substrate material.[43−48] The relationship between the G-band frequency and the Fermi energy was measured for the monolayer graphene on an SiO_2/Si substrate in ref 42. Since the monolayer graphene in our sample is transferred on an SiO_2 substrate, the strain-induced shift in this study is thought to be equivalent to that in the monolayer graphene in ref 42.[49] The Raman spectrum measured for the fresh graphene sample transferred onto an SiO_2 substrate showed the G-band peak at 1583 cm^{-1}, which is the same value as that observed for $|\Delta E_F| < 0.04$ eV in ref 42 (for details, see the Supporting Information). Therefore, we estimate ΔE_F in our graphene sample by referring to ref 42.

Figure 1b shows the Raman spectra measured at six different points separated from each other by ∼2 mm around the center of the graphene sample in the G-band region. The black lines represent the results of curve fitting with a Lorentz function and linear background component, and the peak positions of the Lorentz functions in respective curves are indicated in the figure, the average of which is 1590 cm^{-1}. The estimated ΔE_F is 0.225 eV.[42] Since graphene on an SiO_2 substrate in air is known to be p-doped from the oxygen and moisture in air,[33] our graphene is most probably p-type. Therefore, ΔE_F is determined to be −0.225 eV, corresponding to a hole density of 3.8×10^{16} m^{-2}. It should be noted here that the analysis and discussion in this study are independent of whether the doped carriers are holes or electrons because of symmetrical energy band structures of electrons and holes in graphene.

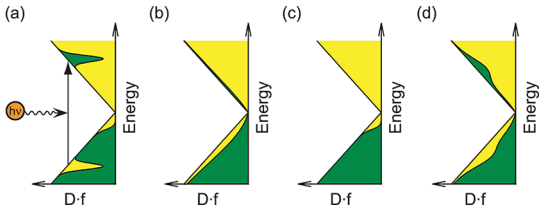

Figure 3. Schematics of time evolution of the distribution functions of an electron (f_e) and hole (f_h) weighted by the density of states (D). (a) Under pulse excitation. (b) After thermalization of carriers. (c) During cooling to room temperature. (d) On the way to thermalization. Thermalization of the carrier distributions is not fully achieved, i.e., non-thermal carriers remain.

The luminescence kinetics in graphene at room temperature in air were measured using femtosecond time-resolved luminescence spectroscopy based on the frequency up-conversion technique[50,51] by employing a mode-locked Ti:sapphire laser (82 MHz, 800 nm, and 100 fs). The excitation density at 800 nm was 3.8×10^{-2} J m^{-2} per pulse. Since the transmission at 800 nm is 97.7%,[52−55] the absorbed pulse energy and photon number are estimated to be 8.7×10^{-4} J m^{-2} and 3.5×10^{15} m^{-2}, respectively. Thus, the number of photoexcited electron−hole pairs is 3.5×10^{15} m^{-2}, an order of magnitude smaller than the number of the doped holes.

Figure 2 shows the observed luminescence kinetics in the photon energy range of 0.7−1.4 eV. For display clarity, the baselines are shifted and the intensities are normalized at the maxima. The luminescence kinetics show longer decay behavior as the photon energy decreases. Above 1.2 eV, the luminescence kinetics show ultrafast decay similar to the instrument response function (cross-correlation trace of the laser pulse; the width of the trace is 140 fs, as shown in the top panel of Figure 2). At 1.0 and 1.1 eV, decay behavior is observed, and the intensity becomes approximately zero in ∼300 fs. Below 0.9 eV, the luminescence kinetics show longer decay; the luminescence decay lasts over 300 fs. Although the decay behavior is not exponential decay, we obtain time constants as a measure of decay time by approximately fitting the measured decay curves to a double-exponential function; the fast and slow time constants are 60 and 360 fs for 0.9 eV, 60 and 530 fs for 0.8 eV, and 90 fs and 1.1 ps for 0.7 eV, respectively. The photon-energy-dependent decay behavior reflects the cooling dynamics of photoexcited carriers, which is qualitatively explained in Figure 3. Figure 3 shows schematics of the time evolution of the Fermi−Dirac distribution functions of an electron (f_e) and hole (f_h) weighted by the density of states D ($D(E) = (2|E|/\pi)/(\hbar v_F)^2$ with the Fermi velocity v_F of 1.1×10^6 m s^{-1} (refs 56 and 57), and the origin of energy is set at the Dirac

point). The laser pulse excites electrons and holes in the linear dispersion bands (Figure 3a). Due to carrier−carrier scattering, thermalization within the carrier system is achieved (Figure 3b). During the thermalization, carrier cooling may partially occur by ultrafast carrier−phonon scattering, if the carrier−phonon interaction is sufficiently strong.[22,27] Cooling of the thermalized carriers occurs with emission of phonons *via* carrier−phonon interactions (Figure 3c). Consequently, the value of the weighted distribution function $f_{e,h}D$ at a high energy decreases faster than at a low energy. As the luminescence intensity at photon energy $\hbar\omega$ is proportional to the product of $f_e(\hbar\omega/2)D(\hbar\omega/2)$ and $f_h(\hbar\omega/2)D(-\hbar\omega/2)$ (details will be described later), the luminescence at high photon energy decays faster than that at low photon energy.

In order to quantitatively discuss the carrier dynamics, we analyze the observed luminescence kinetics using model calculations. We assume that the carrier system is instantaneously thermalized by the ultrafast carrier−carrier scattering, and the carrier temperature is defined at any time. First, the luminescence intensity at the photon energy $\hbar\omega$ for the radiative recombination of free electron−hole pairs is given by Fermi's golden rule:

$$f_e(\hbar\omega/2, \mu_e, T_e)\, D(\hbar\omega/2)\, f_h(\hbar\omega/2, \mu_h, T_h)\, D(-\hbar\omega/2)(\hbar\omega)^3 \quad (1)$$

Here, the electron temperature T_e is equal to the hole temperature T_h and the chemical potential $|\mu_e| = |\mu_h|$, since we assume ultrafast scattering between electrons and holes. Consequently, $f_h(\hbar\omega/2,\mu_h,T_h) = 1 - f_e(-\hbar\omega/2,\mu_e,T_e)$. In eq 1, $(\hbar\omega)^3$ expresses the probability of spontaneous emission, which is proportional to the cube of the photon energy. As the electron temperature varies with time, the luminescence intensity is a function of time.

The time evolution of the electron temperature is calculated in the following way. We consider the two-temperature model[58,59] taking into account the carrier−phonon interactions. Energy relaxation processes in graphene due to surface polar phonon mode of the substrate as well as intrinsic optical and acoustic phonons have been discussed for electronic transport[60,61] and photoexcited carrier cooling.[9,13,62] The studies on carrier cooling in the femtosecond time region showed that the dominant contribution to cooling is the coupling to optical and acoustic phonons in graphene. In 1−4-layer and 10-layer CVD-grown graphene transferred onto SiO_2 substrates, the rise and decay kinetics of differential transmission spectra show similar behavior and are independent of the number of layers.[63] This result indicates that the surface polar phonon mode plays a less important role in the initial process of hot electron cooling under ultrafast laser excitations in the transferred graphene. Similar results have been reported for monolayer graphene on SiO_2 and mica substrates,[15] and monolayer and multilayer graphene on SiC and glass substrates.[64] Hence, we take intrinsic phonons in graphene that couple to carriers.

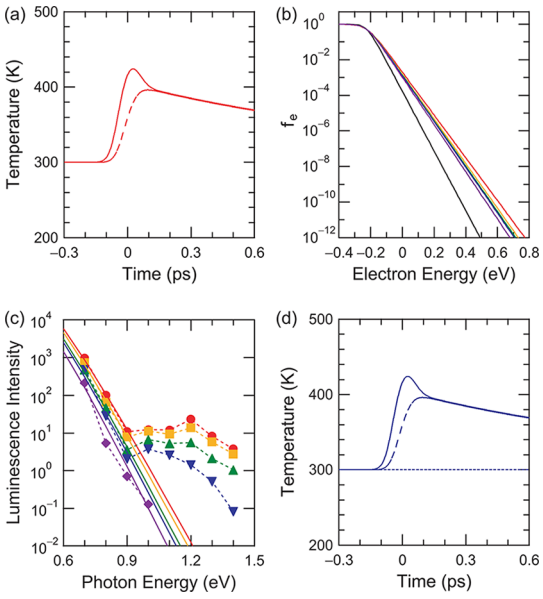

Figure 4. (a) Time evolutions of electron and optical-phonon temperatures calculated using the two-temperature model. The solid and dashed curves represent the electron and optical-phonon temperatures, respectively. (b) Time evolution of the Fermi−Dirac distribution function calculated using the two-temperature model: From top to bottom, the distribution functions at 50, 100, 150, 200, and 400 fs, and the bottom curve (black) represents the distribution function before the pulse excitation. (c) Time evolution of the luminescence spectrum. The solid curves represent the luminescence spectra calculated using the two-temperature model. From top to bottom, plotted curves represent the spectra at 50, 100, 150, 200, and 400 fs. The symbols represent experimental data: 50 fs (○), 100 fs (□), 150 fs (△), 200 fs (▽), and 400 fs (◇). The experimental error of the luminescence intensity is 10% at each photon energy. (d) Time evolutions of the electron, optical-phonon, and acoustic-phonon temperatures calculated using the three-temperature model. The solid, dashed, and dotted curves represent the electron, optical-phonon, and acoustic-phonon temperatures, respectively.

Since optical phonons strongly couple to carriers,[65−67] the carrier−optical phonon interaction is taken into account in the present model. Referring to the paper by Lui *et al.*,[15] the time evolution of the electron (T_e) and optical phonon (T_p) temperatures is described by the following rate equations:

$$[C_e(T_e) + C_h(T_e)]\frac{dT_e}{dt} = I - \Gamma(T_e, T_p) \quad (2)$$

$$C_p(T_p)\frac{dT_p}{dt} = \Gamma(T_e, T_p) - C_p(T_p)\frac{T_p - T_0}{\tau_p} \quad (3)$$

Here, C_e, C_h, and C_p are the specific heats of electrons, holes, and optical phonons, respectively. Due to the symmetrical energy band structures of electrons and holes, $C_e \approx C_h$. C_e is calculated from the expression for electron energy near the Fermi energy.[19] C_p is calculated by assuming the optical phonons to be Einstein

phonons. In the calculation, the filling fraction of the optical phonons in the Brillouin zone is estimated by fitting C_p to the derivative of the empirical relationship between the optical phonon temperature and the energy density of the graphene layer.[68,69] I is the laser pulse trace, which has a Gaussian shape with a full width at half-maximum of 100 fs and an area with absorbed pulse energy of 8.7×10^{-4} J m^{-2}. $\Gamma(T_e,T_p)$ is the rate of carrier−phonon scattering, resulting in energy flow between the carrier and phonon systems. Assuming the optical phonons to be the Einstein phonons, the rates of emission and absorption of phonons are calculated with the coupling constant of 5×10^{-4} eV^2 m^2 s^{-1}.[15] Cooling of the optical-phonon system occurs with emission of low-energy phonons in both the graphene and the substrate. As the specific heat of acoustic phonons is high, secondary-phonon systems are considered as a heat bath in this model. The cooling term of the optical-phonon system is expressed by the last term in eq 3. T_0 is the room temperature (300 K), and τ_p is the lifetime of optical phonons, estimated to be 1.2 ps by time-resolved Raman scattering measurements.[71]

The time evolutions of T_e and T_p are obtained by numerically solving eqs 2 and 3, as shown in Figure 4a. Before the laser pulse excitation, T_e and T_p are fixed to be constant at room temperature. At −0.1 ps, the tail of the laser pulse penetrates into the graphene sample. Up to 0 ps, the laser pulse propagates in the sample with its instantaneous intensity increasing and heats the carrier system at the temperature of T_e. Following T_e, the phonon temperature T_p increases according to $\Gamma(T_e,T_p)$. The maximum value of T_e is 420 K, which is an order of magnitude lower than reported in early work on luminescence measurements.[15] The discrepancy between the obtained maximum temperatures can be attributed to two causes: The excitation pulse energy in our experiments is an order of magnitude lower, and the pulse duration is about an order of magnitude longer than in the previous experiments. After 0 ps, the peak of the laser pulse trace passes through the sample, and its instantaneous intensity decreases. As the inflow energy from the laser pulse to the carrier system falls below the outflow energy to the optical-phonon system, T_e decreases and T_p increases toward T_e, showing saturation behavior. After *ca.* 0.1 ps, both T_e and T_p have the same value. Then, the decrease in T_e slows because the carriers couple to the hot optical phonons, whose temperature slowly decreases to room temperature T_0 (300 K) with a time constant τ_p of 1.2 ps.

Using the time evolution of T_e in Figure 4a, we calculate the time evolution of f_e. Here, μ_e is set at $\Delta E_F = -0.225$ eV, because T_e increases to only 420 K at maximum and is much lower than $|\Delta E_F| = 0.225$ eV (∼2600 K) due to hole doping. Figure 4b shows the calculated result for f_e. The bottom curve represents f_e before the pulse excitation, *i.e.*, f_e at 300 K. After the pulse excitation, at 50 fs (the top curve), a hot distribution is achieved with the rise in T_e. As time proceeds, at 100, 150, 200, and 400 fs (from top to bottom), f_e gradually returns to the distribution before the pulse excitation due to the reduction in T_e.

We can now calculate the time evolution of the luminescence spectrum using eq 1 and the calculated distribution function f_e. Figure 4c shows the calculated time evolution of the luminescence spectrum. The plotted curves from top to bottom represent the spectra at 50, 100, 150, 200, and 400 fs, and the symbols represent experimental data. The calculated results fit the experimental data in the photon energy range 0.7−0.9 eV. In this range, the luminescence kinetics in Figure 2 are also reproduced well by the calculated curves (solid curves): (1) The fast decay reflecting the cooling of T_e until T_p becomes equal to T_e at ∼0.1 ps and (2) the subsequent long decay reflecting the bottleneck of the hot phonons, which cool with a time constant of 1.2 ps. While good agreement between the calculations and experiments is obtained in the range 0.7−0.9 eV, a weak luminescence tail is observed in the photon energy range 1.0−1.4 eV in the experiments. This high-energy luminescence cannot be reproduced by the calculations with any set of parameters, for example, a smaller coupling constant of the carrier−phonon interaction. Consequently, the model analysis based on the assumption that the photoexcited carriers are instantaneously thermalized is not adequate for explanation of the carrier cooling dynamics, and the existence of nonthermal carriers in the high-energy region is suggested. Since the luminescence intensities at 1.0 and 1.1 eV last for ∼300 fs, as shown in Figure 2, thermalization of the carrier system is not completed by ∼300 fs. A possible origin of the lasting nonthermal carriers is carriers excited in the energy region above the linear dispersion relation. Since two-photon absorption should not occur under our excitation density according to the early studies,[15,16] the high-energy carriers are excited by scattering between photoexcited carriers assisted by phonons for energy-momentum conservation. The energy of scattered carriers, *e.g.*, $0.75 \times 2 = 1.5$ eV (optical transition energy $1.5 \times 2 = 3.0$ eV), lies in the region of the nonlinear dispersion relation approaching the saddle point (M point).[27] Although the scattering rate might be low, once the carriers are excited in the nonlinear dispersion region, their relaxation is relatively slow, and thus the nonthermal carriers remain for several hundreds of femtoseconds.

Here, we discuss the difference in spectral shape between our study and the early studies. In the exfoliated monolayer graphene[15,16] the luminescence spectra were observed in the energy range above

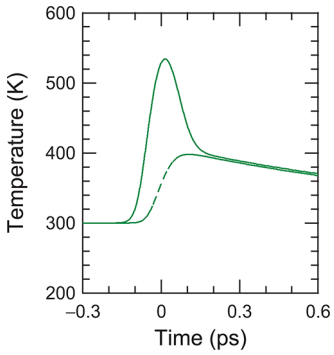

Figure 5. Time evolutions of electron and optical-phonon temperatures calculated using the two-temperature model without the Fermi energy shift (undoped graphene). The solid and dashed curves represent the electron and optical-phonon temperatures, respectively.

~1.7 eV when the samples were excited at 1.5 eV with shorter and more intense pulses than those of our case. The observed spectra show a monotonous decrease with increasing photon energy, and spectral tails are observed even in the near-ultraviolet region; the luminescence intensity at 3.0 eV is ~7% of the intensity at 1.7 eV.[15] This spectral behavior can be explained in terms of the thermal radiation.[15] The dependence of total radiant fluence on the absorbed fluence F for $F > 0.2$ J m^{-2} is well reproduced by the calculation based on the two-temperature model. However, for $F < 0.2$ J m^{-2}, the experimental value is larger than the calculated one, and the discrepancy increases with decreasing absorbed fluence, suggesting the existence of another luminescence component. In our study, the graphene sample was excited at 1.55 eV with the weak laser pulse (~8.7×10^{-4} J m^{-2}), and the luminescence was observed in the spectral range 0.7−1.4 eV. As shown in Figure 4c, the spectral shape observed in our study is much sharper than those in the early studies; the luminescence intensity at 0.9 eV is only ~1% of that at 0.7 eV. The sharp spectral width is due to the low maximum temperature of carriers, leading to a narrow width of the Fermi distribution function. A striking difference from the spectral shape observed in the early studies is the existence of the luminescence tail above 1.0 eV, which suggests the lasting nonthermal carriers. At the low absorbed fluence, the intensity of the nonthermal carrier component relative to that of the thermal radiation becomes high. This is the reason that the nonthermal carrier component is observed in our study. In ref 15, this component may be seen as a deviation from the calculation when the absorbed fluence is lower than ~0.2 J m^{-2}.

Next, we discuss the importance of the Fermi energy shift due to carrier doping for the luminescence kinetics. The luminescence kinetics were calculated using the two-temperature model under the condition of no carrier doping, *i.e.*, $\Delta E_F = 0$, and the results are shown by the dashed lines in Figure 2. The calculated luminescence kinetics decay fast, even in the range 0.7−0.9 eV, and the experimental data cannot be reproduced. However, if we magnify the calculated curves for $\Delta E_F = 0$ by 100 times, the results (dashed lines) correspond well to those for $\Delta E_F = -0.225$ eV (solid lines) after ~200 fs. Such dynamical behavior originates from the time evolution of T_e. The time evolution of T_e, shown in Figure 5, is calculated using the two-temperature model for $\Delta E_F = 0$. T_e increases up to ~530 K just after the time origin and quickly decreases to ~400 K in 200 fs. After 200 fs, the decrease of T_e exhibits the same behavior as that observed in doped graphene (Figure 4a); the slow decrease is due to the coupling of carriers to the hot optical phonons. The maximum value of T_e ~530 K is higher than ~420 K in our experiments, because the heat capacity of electrons in undoped graphene is smaller because of the lower density of states around the Dirac point. Due to the higher maximum value of T_e, the luminescence intensity around the time origin is higher. Since the values of T_e in both calculations are the same after 200 fs, the luminescence kinetics show the same behavior. Consequently, our experiments and model calculations clearly show that the carrier doping effect should be considered in the optical responses in graphene, which has electron heat capacity sensitive to carrier doping due to the linear dispersion bands contacting each other at the Dirac point.

Finally, the contribution of acoustic phonons to the carrier cooling is discussed. We performed the calculation based on the three-temperature model, taking into account the interaction between carriers and acoustic phonons as well as optical phonons. Following ref 29, the coupling of carriers to acoustic phonons with linear energy dispersion is considered. In the carrier-doped graphene, wherein μ_e is higher than T_e (highly doped limit), the differential of T_e caused by the carrier-acoustic phonon coupling is written in the form $\gamma_d(T_e - T_a)/T_e$.[29] Here, $\gamma_d = 0.133D^2n^{3/2}$ meV ns^{-1}, where D is the deformation potential measured in units of eV, n is the carrier density measured in terms of 10^{12} cm^{-2}, and T_a is the acoustic phonon temperature. Thus, we add this coupling term in eq 2. Using the values of $D = 20$ eV (ref 29), $n = 3.8$ (as determined by the G-band frequency in the Raman spectra in Figure 1b), and the estimated specific heat of acoustic phonons is obtained by the polynomial fit to the first principle calculation[70] in the low-temperature region, T_e, T_p, and T_a are calculated and plotted in Figure 4d. The obtained time evolution of T_e is almost the same as that obtained using the two-temperature model without taking into account the carrier−acoustic phonon coupling. Therefore, carrier cooling by the coupling to the acoustic phonons is negligible, and the coupling to the optical phonons is predominant in the carrier cooling even at the electron temperature of ~400 K.

CONCLUSION

We experimentally investigated the carrier dynamics in single-monolayer graphene on an SiO_2 substrate at room temperature in air using femtosecond time-resolved luminescence measurements. The luminescence kinetics were observed in the near-infrared region of 0.7−1.4 eV and analyzed based on the carrier cooling model, *i.e.*, the two-temperature model taking into account the carrier−optical phonon interaction. While the observed luminescence in the range 0.7−0.9 eV is well reproduced by the model, the weak luminescence decaying within ∼300 fs in the range 1.0−1.4 eV cannot be reproduced by this model. These results indicate that the carrier system is in nearly thermal equilibrium, but is not completely thermalized in ∼300 fs. Furthermore, our analysis revealed the importance of the carrier-doping effect in the cooling dynamics of photoexcited carriers. We also showed that carrier−optical phonon coupling is predominant over carrier−acoustic phonon coupling in the carrier-cooling process at a temperature of ∼400 K.

EXPERIMENTAL METHODS

The monolayer graphene samples used in this study were epitaxially grown on Cu(111)/sapphire by chemical vapor deposition. Details of the growth are described in refs 36−38. In brief, Cu films (500 nm thickness) were deposited onto a *c*-plane sapphire substrate in an Ar gas atmosphere (0.6 Pa) by sputtering. Graphene films were grown on the Cu film by chemical vapor deposition at 1000 °C for 10 min under ambient pressure with a gas flow of CH_4/H_2/Ar (volume ratio, 0.4/2.0/97.6) and then rapidly cooled to room temperature in an H_2/Ar flow. The obtained graphene films were transferred as follows. The graphene film on the Cu(111)/sapphire substrate was covered with polymethyl methacrylate (PMMA) by a spin-coating technique. The Cu film was then dissolved in a $FeCl_3$/HCl aqueous solution. The thus released graphene film on PMMA was washed with deionized water and transferred onto an SiO_2 substrate. Finally, the PMMA was removed by acetone, leaving the graphene film on the SiO_2 substrate.

Raman spectra were measured by a Renishaw spectrometer with a He−Ne laser at 632.8 nm and a 50× objective lens (spot size ∼4 μm). Since no spectral change was observed for excitation densities of 8.8×10^5 to 8.8×10^6 W m^{-2}, laser-induced damage and heating were avoided for these excitation densities. The Raman spectra shown in this paper were measured with the excitation density of 8.8×10^6 W m^{-2} at room temperature in air.

Luminescence kinetics were measured using femtosecond time-resolved luminescence spectroscopy based on the frequency up-conversion technique.[50,51] The light source was a mode-locked Ti:sapphire laser (82 MHz, 800 nm, and 100 fs), and the excitation density was 3.8×10^{-2} J m^{-2} per pulse (1.5×10^{17} photons m^{-2} per pulse). The instrument response function of the measurement system was determined by measuring the cross-correlation trace between the gate pulse and excitation pulse, which had a Gaussian shape with a full width at half-maximum of 140 fs. The spectral resolution was about 0.03 eV. As described in the Supporting Information of refs 72 and 73, we detected background signals in the frequency up-conversion measurements, which were observed even in the range of negative time delay, due to the un-phase-matched second harmonics of the strong gate pulse and other stray light. To obtain the luminescence signal component, we subtracted the average signal level in the negative time range from the measured signal of the decay curve. Time-resolved luminescence measurements were conducted at room temperature in air.

Conflict of Interest: The authors declare no competing financial interest.

Acknowledgment. This work was supported by KAKENHI (Grant Nos. 21740225 and 21340081) and the JSPS Funding Program for Next Generation World-Leading Researchers.

Supporting Information Available: Additional data on Raman spectra. This material is available free of charge *via* the Internet at http://pubs.acs.org.

REFERENCES AND NOTES

1. Geim, A. K.; Novoselov, K. S. The Rise of Graphene. *Nat. Mater.* **2007**, *6*, 183–191.
2. Castro Neto, A. H.; Guinea, F.; Peres, N. M. R.; Novoselov, K. S.; Geim, A. K. The Electronic Properties of Graphene. *Rev. Mod. Phys.* **2009**, *81*, 109–162.
3. Abergel, D. S. L.; Apalkov, V.; Berashevich, J.; Ziegler, K.; Chakraborty, T. Properties of Graphene: A Theoretical Perspective. *Adv. Phys.* **2010**, *59*, 261–482.
4. Avouris, Ph. Graphene: Electronic and Photonic Properties and Devices. *Nano Lett.* **2010**, *10*, 4285–4294.
5. Das Sarma, S.; Adam, S.; Hwang, E. H.; Rossi, E. Electronic Transport in Two-Dimensional Graphene. *Rev. Mod. Phys.* **2011**, *83*, 407–470.
6. Dawlaty, J. M.; Shivaraman, S.; Chandrashekhar, M.; Rana, F.; Spencer, M. G. Measurement of Ultrafast Carrier Dynamics in Epitaxial Graphene. *Appl. Phys. Lett.* **2008**, *92*, 042116.
7. Sun, D.; Wu, Z.-K.; Divin, C.; Li, X.; Berger, C.; de Heer, W. A.; First, P. N.; Norris, T. B. Ultrafast Relaxation of Excited Dirac Fermions in Epitaxial Graphene Using Optical Differential Transmission Spectroscopy. *Phys. Rev. Lett.* **2008**, *101*, 157402.
8. George, P. A.; Strait, J.; Dawlaty, J.; Shivaraman, S.; Chandrashekhar, M.; Rana, F.; Spencer, M. G. Ultrafast Optical-Pump Terahertz-Probe Spectroscopy of the Carrier Relaxation and Recombination Dynamics in Epitaxial Graphene. *Nano Lett.* **2008**, *8*, 4248–4251.
9. Newson, R. W.; Dean, J.; Schmidt, B.; van Driel, H. M. Ultrafast Carrier Kinetics in Exfoliated Graphene and Thin Graphite Films. *Opt. Express* **2009**, *17*, 2326–2333.
10. Kumar, S.; Anija, M.; Kamaraju, N.; Vasu, K. S.; Subrahmanyam, K. S.; Sood, A. K.; Rao, C. N. R. Femtosecond Carrier Dynamics and Saturable Absorption in Graphene Suspensions. *Appl. Phys. Lett.* **2009**, *95*, 191911.
11. Wang, H.; Strait, J. H.; George, P. A.; Shivaraman, S.; Shields, V. B.; Chandrashekhar, M.; Hwang, J.; Rana, F.; Spencer, M. G.; Ruiz-Vargas, C. S.; *et al*. Ultrafast Relaxation Dynamics of Hot Optical Phonons in Graphene. *Appl. Phys. Lett.* **2010**, *96*, 081917.
12. Plochocka, P.; Kossacki, P.; Golnik, A.; Kazimierczuk, T.; Berger, C.; de Heer, W. A.; Potemski, M. Slowing Hot-Carrier Relaxation in Graphene Using a Magnetic Field. *Phys. Rev. B* **2009**, *80*, 245415.
13. Huang, L.; Hartland, G. V.; Chu, L.-Q.; Luxmi; Feenstra, R. M.; Lian, C.; Tahy, K.; Xing, H. Ultrafast Transient Absorption Microscopy Studies of Carrier Dynamics in Epitaxial Graphene. *Nano Lett.* **2010**, *10*, 1308–1313.
14. Xing, G.; Guo, H.; Zhang, X.; Sum, T. C.; Huan, C. H. A. The Physics of Ultrafast Saturable Absorption in Graphene. *Opt. Express* **2010**, *18*, 4564–4573.
15. Lui, C. H.; Mak, K. F.; Shan, J.; Heinz, T. F. Ultrafast Photoluminescence from Graphene. *Phys. Rev. Lett.* **2010**, *105*, 127404.
16. Liu, W.-T.; Wu, S. W.; Schuck, P. J.; Salmeron, M.; Shen, Y. R.; Wang, F. Nonlinear Broadband Photoluminescence of Graphene Induced by Femtosendo Laser Irradiation. *Phys. Rev. B* **2010**, *82*, 081408(R).

17. Zou, X.; Zhan, D.; Fan, X.; Lee, D.; Nair, S. K.; Sun, L.; Ni, Z.; Luo, Z.; Liu, L.; Yu, T.; *et al*. Ultrafast Carrier Dynamics in Pristine and $FeCl_3$-Intercalated Bilayer Graphene. *Appl. Phys. Lett.* **2010**, *97*, 141910.
18. Shang, J.; Luo, Z.; Cong, C.; Lin, J.; Yu, T.; Gurzadyan, G. G. Femtosecond UV-Pump/Visible-Probe Measurements of Carrier Dynamics in Stacked Graphene Films. *Appl. Phys. Lett.* **2010**, *97*, 163103.
19. Sun, D.; Divin, C.; Berger, C.; de Heer, W. A.; First, P. N.; Norris, T. B. Hot Carrier Cooling by Acoustic Phonons in Epitaxial Graphene by Ultrafast Pump-Probe Spectroscopy. *Phys. Status Solidi C* **2011**, *8*, 1194–1197.
20. Obraztsov, P. A.; Rybin, M. G.; Tyurnina, A. V.; Garnov, S. V.; Obraztsova, E. D.; Obraztsov, A. N.; Svirko, Y. P. Broadband Light-Induced Absorbance Change in Multilayer Graphene. *Nano Lett.* **2011**, *11*, 1540–1545.
21. Strait, J. H.; Wang, H.; Shivaraman, S.; Shields, V.; Spencer, M.; Rana, F. Very Slow Cooling Dynamics of Photoexcited Carriers in Graphene Observed by Optical-Pump Terahertz-Probe Spectroscopy. *Nano Lett.* **2011**, *11*, 4902–4906.
22. Breusing, M.; Kuehn, S.; Winzer, T.; Malić, E.; Milde, F.; Severin, N.; Rabe, J. P.; Ropers, C.; Knorr, A.; Elsaesser, T. Ultrafast Nonequilibrium Carrier Dynamics in a Single Graphene Layer. *Phys. Rev. B* **2011**, *83*, 153410.
23. Yang, H.; Feng, X.; Wang, Q.; Huang, H.; Chen, W.; Wee, A. T. S.; Ji, W. Giant Two-Photon Absorption in Bilayer Graphene. *Nano Lett.* **2011**, *11*, 2622–2627.
24. Butscher, S.; Milde, F.; Hirtschulz, M.; Malić, E.; Knorr, A. Hot Electron Relaxation and Phonon Dynamics in Graphene. *Appl. Phys. Lett.* **2007**, *91*, 203103.
25. Winzer, T.; Knorr, A.; Malic, E. Carrier Multiplication in Graphene. *Nano Lett.* **2010**, *10*, 4839–4843.
26. Kim, R.; Perebeinos, V.; Avouris, Ph. Relaxation of Optically Excited Carriers in Graphene. *Phys. Rev. B* **2011**, *84*, 075449.
27. Malic, E.; Winzer, T.; Bobkin, E.; Knorr, A. Microscopic Theory of Absorption and Ultrafast Many-Particle Kinetics in Graphene. *Phys. Rev. B* **2011**, *84*, 205406.
28. Tse, W.-K.; Das Sarma, S. Energy Relaxation of Hot Dirac Fermions in Graphene. *Phys. Rev. B* **2009**, *79*, 235406.
29. Bistritzer, R.; MacDonald, A. H. Electronic Cooling in Graphene. *Phys. Rev. Lett.* **2009**, *102*, 206410.
30. Romero, H. E.; Shen, N.; Joshi, P.; Gutierrez, H. R.; Tadigadapa, S. A.; Sofo, J. O.; Eklund, P. C. n-Type Behavior of Graphene Supported on Si/SiO_2 Substrates. *ACS Nano* **2008**, *2*, 2037–2044.
31. Shi, Y.; Dong, X.; Chen, P.; Wang, J.; Li, L.-J. Effective Doping of Single-Layer Graphene from Underlying SiO_2 Substrates. *Phys. Rev. B* **2009**, *79*, 115402.
32. Joshi, P.; Romero, H. E.; Neal, A. T.; Toutam, V. K.; Tadigadapa, S. A. Intrinsic Doping and Gate Hysteresis in Graphene Field Effect Devices Fabricated on SiO_2 Substrates. *J. Phys. C* **2010**, *22*, 334214.
33. Ryu, S.; Liu, L.; Berciaud, S.; Yu, Y.-J.; Liu, H.; Kim, P.; Flynn, G. W.; Brus, L. E. Atmospheric Oxygen Binding and Hole Doping in Deformed Graphene on a SiO_2 Substrate. *Nano Lett.* **2010**, *10*, 4944–4951.
34. Crowther, A. C.; Ghassaei, A.; Jung, N.; Brus, L. E. Strong Charge-Transfer Doping of 1 to 10 Layer Graphene by NO_2. *ACS Nano* **2012**, *6*, 1865–1875.
35. Gilbertson, S.; Dakovski, G. L.; Durakiewicz, T.; Zhu, J.-X.; Dani, K. M.; Mohite, A. D.; Dattelbaum, A.; Rodriguez, G. Tracing Ultrafast Separation and Coalescence of Carrier Distributions in Graphene with Time-Resolved Photoemission. *J. Phys. Chem. Lett.* **2012**, *3*, 64–68.
36. Hu, B.; Ago, H.; Ito, Y.; Kawahara, K.; Tsuji, M.; Magome, E.; Sumitani, K.; Mizuta, N.; Ikeda, K.; Mizuno, S. Epitaxial Growth of Large-Area Single-Layer Graphene over Cu(111)/Sapphire by Atmospheric Pressure CVD. *Carbon* **2012**, *50*, 57–65.
37. Orofeo, C. M.; Hibino, H.; Kawahara, K.; Ogawa, Y.; Tsuji, M.; Ikeda, K.; Mizuno, S.; Ago, H. Influence of Cu Metal on the Domain Structure and Carrier Mobility in Single-Layer Graphene. *Carbon* **2012**, *50*, 2189–2196.
38. Ago, H.; Ogawa, Y.; Tsuji, M.; Mizuno, S.; Hibino, H. Catalytic Growth of Graphene: Toward Large-Area Single-Crystalline Graphene. *J. Phys. Chem. Lett.* **2012**, *3*, 2228–2236.
39. Jorio, A.; Dresselhaus, M. S.; Saito, R.; Dresselhaus, G. F. *Raman Spectroscopy in Graphene Related Systems*; Wiley-VCH: Weinheim, 2011.
40. Ferrari, A. C.; Meyer, J. C.; Scardaci, V.; Casiraghi, C.; Lazzeri, M.; Mauri, F.; Piscanec, S.; Jiang, D.; Novoselov, K. S.; Roth, S.; *et al*. Raman Spectrum of Graphene and Graphene Layers. *Phys. Rev. Lett.* **2006**, *97*, 187401.
41. Reina, A.; Jia, X.; Ho, J.; Nezich, D.; Son, H.; Bulovic, V.; Dresselhaus, M. S.; Kong, J. Large Area, Few-Layer Graphene Films on Arbitrary Substrates by Chemical Vapor Deposition. *Nano Lett.* **2009**, *9*, 30–35.
42. Yan, J.; Zhang, Y.; Kim, P.; Pinczuk, A. Electric Field Effect Tuning of Electron-Phonon Coupling in Graphene. *Phys. Rev. Lett.* **2007**, *98*, 166802.
43. Ni, Z. H.; Chen, W.; Fan, X. F.; Kuo, J. L.; Yu, T.; Wee, A. T. S.; Shen, Z. X. Raman Spectroscopy of Epitaxial Graphene on a SiC Substrate. *Phys. Rev. B* **2008**, *77*, 115416.
44. Ferralis, N.; Maboudian, R.; Carraro, C. Evidence of Structural Strain in Epitaxial Graphene Layers on 6H-SiC(0001). *Phys. Rev. Lett.* **2008**, *101*, 156801.
45. Berciaud, S.; Ryu, S.; Brus, L. E.; Heinz, T. F. Probing the Intrinsic Properties of Exfoliated Graphene: Raman Spectroscopy of Free-Standing Monolayers. *Nano Lett.* **2009**, *9*, 346–352.
46. Yu, V.; Whiteway, E.; Maassen, J.; Hilke, M. Raman Spectrosocpy of the Internal Strain of a Graphene Layer Grown on Copper Tuned by Chemical Vapor Deposition. *Phys. Rev. B* **2011**, *84*, 205407.
47. Lee, J. E.; Ahn, G.; Shim, J.; Lee, Y. S.; Ryu, S. Optical Separation of Mechanical Strain from Charge Doping in Graphene. *Nature Commun.* **2012**, *3*, 1024.
48. Bissett, M. A.; Izumida, W.; Saito, R.; Ago, H. Effect of Domain Boundaries on the Raman Spectra of Mechanically Strained Graphene. *ACS Nano* **2012**, *6*, 10229–10238.
49. Wang, Y. Y.; Ni, Z. H.; Yu, T.; Shen, Z. X.; Wang, H. M.; Wu, Y. H.; Chen, W.; Wee, A. T. S. Raman Studies of Monolayer Graphene: The Substrate Effect. *J. Phys. Chem. C* **2008**, *112*, 10637–10640.
50. Koyama, T.; Suemoto, T. Dynamics of Nuclear Wave Packets at the *F* Center in Alkali Halides. *Rep. Prog. Phys.* **2011**, *74*, 076502.
51. Koyama, T.; Miyata, Y.; Asaka, K.; Shinohara, H.; Saito, Y.; Nakamura, A. Ultrafast Energy Transfer of One-Dimensional Excitons between Carbon Nanotubes: A Femtosecond Time-Resolved Luminescence Study. *Phys. Chem. Chem. Phys.* **2012**, *14*, 1070–1084.
52. Ando, T.; Zheng, Y.; Suzuura, H. Dynamical Conductivity and Zero-Mode Anomaly in Honeycomb Lattices. *J. Phys. Soc. Jpn.* **2002**, *71*, 1318–1324.
53. Kuzmenko, A. B.; van Heumen, E.; Carbone, F.; van der Marel, D. Universal Optical Conductance of Graphite. *Phys. Rev. Lett.* **2008**, *100*, 117401.
54. Nair, R. R.; Blake, P.; Grigorenko, A. N.; Novoselov, K. S.; Booth, T. J.; Stauber, T.; Peres, N. M. R.; Geim, A. K. Fine Structure Constant Defined Visual Transparency of Graphene. *Science* **2008**, *320*, 1308.
55. Mak, K. F.; Sfeir, M. Y.; Wu, Y.; Lui, C. H.; Misewich, J. A.; Heinz, T. F. Measurement of the Optical Conductivity of Graphene. *Phys. Rev. Lett.* **2008**, *101*, 196405.
56. Novoselov, K. S.; Geim, A. K.; Morozov, S. V.; Jiang, D.; Katsnelson, M. I.; Grigorieva, I. V.; Dubonos, S. V.; Firsov, A. A. Two-Dimensional Gas of Massless Dirac Fermions in Graphene. *Nature* **2005**, *438*, 197–200.
57. Zhang, Y.; Tan, Y.-W.; Stormer, H. L.; Kim, P. Experimental Observation of the Quantum Hall Effect and Berry's Phase in Graphene. *Nature* **2005**, *438*, 201–204.
58. Anisimov, S. I.; Kapeliovich, B. L.; Perel'man, T. L. Electron Emission from Metal Surfaces Exposed to Ultrashort Laser Pulses. *Zh. Eksp. Teor. Fiz.* **1974**, *66*, 776–781; *Sov. Phys. JETP* **1974**, *39*, 375–377.
59. Allen, P. B. Theory of Thermal Relaxation of Electrons in Metals. *Phys. Rev. Lett.* **1987**, *59*, 1460–1463.
60. Fratini, S.; Guinea, F. Substrate-Limited Electron Dynamics in Graphene. *Phys. Rev. B* **2008**, *77*, 195415.

61. Freitag, M.; Steiner, M.; Martin, Y.; Perebeinos, V.; Chen, Z.; Tsang, J. C.; Avouris, Ph. Energy Dissipation in Graphene Field-Effect Transistors. *Nano Lett.* **2009**, *9*, 1883–1888.
62. Low, T.; Perebeinos, V.; Kim, R.; Freitag, M.; Avouris, Ph. Cooling of Photoexcited Carriers in Graphene by Internal and Substrate Phonons. *Phys. Rev. B* **2012**, *86*, 045413.
63. Shang, J.; Yu, T.; Lin, J.; Gurzadyan, G. G. Ultrafast Electron-Optical Phonon Scattering and Quasiparticle Lifetime in CVD-Grown Graphene. *ACS Nano* **2011**, *5*, 3278–3283.
64. Huang, L.; Gao, B.; Hartland, G.; Kelly, M.; Xing, H. Ultrafast Relaxation of Hot Optical Phonons in Monolayer and Multilayer Graphene on Different Substrates. *Surf. Sci.* **2011**, *605*, 1657–1661.
65. Maultzsch, J.; Reich, S.; Thomsen, C.; Requardt, H.; Ordejón, P. Phonon Dispersion in Graphite. *Phys. Rev. Lett.* **2004**, *92*, 075501.
66. Piscanec, S.; Lazzeri, M.; Mauri, F.; Ferrari, A. C.; Robertson, J. Kohn Anomalies and Electron-Phonon Interactions in Graphite. *Phys. Rev. Lett.* **2004**, *93*, 185503.
67. Kampfrath, T.; Perfetti, L.; Schapper, F.; Frischkorn, C.; Wolf, M. Strongly Coupled Optical Phonons in the Ultrafast Dynamics of the Electronic Energy and Current Relaxation in Graphite. *Phys. Rev. Lett.* **2005**, *95*, 187403.
68. Yan, H.; Song, D.; Mak, K. F.; Chatzakis, I.; Maultzsch, U.; Heinz, T. F. Time-Resolved Raman Spectroscopy of Optical Phonons in Graphite: Phonon Anharmonic Coupling and Anomalous Stiffening. *Phys. Rev. B* **2009**, *80*, 121403(R).
69. Malard, L. M.; Mak, K. F.; Castro Neto, A. H.; Peres, N. M. R.; Heinz, T. F. Observation of Intra- and Inter-Band Transitions in the Optical Response of Graphene. arXiv:1104.3104, **2011**.
70. Mounet, N.; Marzari, N. First-Principles Determination of the Structural, Vibrational and Thermodynamic Properties of Diamond, Graphite, and Derivatives. *Phys. Rev. B* **2005**, *71*, 205214.
71. Kang, K.; Abdula, D.; Cahill, D. G.; Shim, M. Lifetimes of Optical Phonons in Graphene and Graphite by Time-Resolved Incoherent Anti-Stokes Raman Scattering. *Phys. Rev. B* **2010**, *81*, 165405.
72. Koyama, T.; Asaka, K.; Hikosaka, N.; Kishida, H.; Saito, Y.; Nakamura, A. Ultrafast Exciton Energy Transfer in Bundles of Single-Walled Carbon Nanotubes. *J. Phys. Chem. Lett.* **2011**, *2*, 127–132.
73. Koyama, T.; Shimizu, S.; Saito, T.; Miyata, Y.; Shinohara, H.; Nakamura, A. Ultrafast Luminescence Kinetics of Metallic Single-Walled Carbon Nanotubes: Possible Evidence for Excitonic Luminescence. *Phys. Rev. B* **2012**, *85*, 045428.